IRAQI JOURNAL OF MATERIALS
Volume (4) Issue (4) October-December 2025, pp. 189-198

# Optoelectronics Characteristics of Multilayer $SiC/SiO_2$ and $SiO_2/SiC$ Structures Prepared by DC Reactive Sputtering

**Ruqia A.H. Hassan, Fuad T. Ibrahim**

*Department of Physics, College of Science, University of Baghdad, Baghdad, IRAQ*

**Abstract**
In this work, multilayer heterostructures of $SiC/SiO_2$ and $SiO_2/SiC$ were farbiacted on glass and silicon substrates by dc reactive sputtering technique. The $SiC/SiO_2$ structure shows a spectral responsivity relatively lower as this structure is more sensitive to light in the near-infrared region, which is typical for silicon-based photodetectors due to silicon's bandgap. The $SiO_2/SiC$ structure demonstrates a remarkably higher EQE across almost the entire spectrum reaching about 80% at 400 nm. The $SiO_2/SiC$ structure demonstrates significantly higher detectivity values starting around $0.3\times10^{12}$ Jones at 380 nm, and consistently remains high, peaking at approximately $2.2\times10^{12}$ Jones at 870 nm. This value is several times higher than that of the $SiC/SiO_2$ structure. The dramatically improved detectivity in the $SiO_2/SiC$ configuration suggests a superior signal-to-noise ratio, indicating a more efficient photodetector. This enhanced performance could be attributed to a combination of higher responsivity and lower noise current, possibly stemming from a better-formed junction or reduced defect states at the $SiO_2/SiC$ interface compared to the reverse stacking order. The distinct detectivity profiles clearly illustrate the critical role of layer arrangement in optimizing the performance of these photodetector devices.

***Keywords:*** Optoelectronics; Multilayer structures; Silicon compounds; Reactive sputtering
**Received:** 14 June 2025; **Revised:** 29 July 2025; **Accepted:** 5 August 2025; **Published:** 1 October 2025

## 1. Introduction

Multilayer structures made from silicon compounds offer significant advantages across various fields, particularly in electronics and photonics. A primary benefit is the ability to precisely tune material properties by alternating layers with different compositions or porosity. For instance, in porous silicon, varying the current density during fabrication allows for the creation of layers with different refractive indices, which is essential for manufacturing optical filters, Bragg reflectors, and microcavities [1-3]. This layer-by-layer control enables the creation of devices that can be fine-tuned to specific wavelengths, enhancing their functionality in applications like spectroscopic sensing. Furthermore, silicon compound multilayers provide enhanced thermal and electrical properties [4]. In thermal sensing, multilayered porous silicon nanostructures can be engineered to have a higher thermal resistance at the interfaces between layers, which is crucial for improving device sensitivity [5]. In electronics, these structures can be used to create high-density capacitors with exceptional reliability and stability, even at high temperatures, making them ideal for automotive and aerospace applications [6]. The compatibility of silicon-based multilayer fabrication with existing complementary metal-oxide-semiconductor (CMOS) technology is another key advantage, allowing for the high-density integration of complex components and cost-effective mass production [7]. These benefits make multilayer silicon compound structures a cornerstone of modern technological innovation.

Silicon dioxide ($SiO_2$), commonly known as silica, is a common oxide compound made up of silicon and oxygen atoms bonded together. Within the silica molecules, every silicon atom connects with four oxygen atoms while every oxygen atom connects with two silicon atoms by Si-O bonds [8-10]. This compound is prevalent in various crystalline forms, notably quartz [11], and is also found in amorphous forms such as glass [12]. The basic structural unit of the silicon dioxide is a tetrahedron formed by a silicon atom and four oxygen atoms. The silicon atom sits in the center of the structure and is chemically bonded to the oxygen atoms in the four corners of the tetrahedron. The oxygen atom has two valence electrons, and thus it has a possibility to form a bond to the silicon atom of the neighboring tetrahedron. Since the oxide is amorphous, all of the oxygen atoms do not form bonds between the adjacent structural units. Consequently, depending on the bonding state of the oxygen atoms, they are referred to as bridging or non-bridging oxygen. The amorphous structure forms a more open network and thus the density of the oxide is less than the crystalline form (i.e., the quartz) [13]. $SiO_2$ is characterized by a substantial band gap, this large band gap classifies $SiO_2$ as an insulator, making it an excellent electrical

insulator in various applications [14]. $SiO_2$ nanoparticles are used in various fields, including chemical, biological, and medical applications, due to their chemical stability, optical transparency, low toxicity [15], with low refractive index [16]. It serves as a fundamental component in microelectronics [17], solar cells [18], and protective coatings [19]. $SiO_2$ films are widely used as low-refractive-index layers in multilayer optical devices [20,21], as passivation and protective coatings for silicon devices [22], and as scratch-resistant coatings for plastic ophthalmic lenses [23], and so on. The physical and optical properties of $SiO_2$ layer depend on the method of deposition [24-30]. In reactive sputtering used to prepare nanostructured $SiO_2$ thin films, compound thin films are deposited in the presence of a reactive gas. The reactive gas reacts with the sputtered material and forms a compound. This process makes it possible to deposit a wide variety of compounds (oxides, nitrides, carbides, etc.) with a wide range of properties [31-33]. The ability to deposit high-quality $SiO_2$ thin films with controlled thickness and structural properties is crucial for enhancing the performance of advanced technologies [34-38]. The key parameters influencing the film quality include oxygen partial pressure, DC power, working gas pressure, and substrate temperature, which must be optimized to achieve the desired structural, optical, and electrical properties.

Silicon carbide (SiC) nanostructures are revolutionizing modern electronics and photonics due to their exceptional properties. In electronics, their wide bandgap, high thermal conductivity, and superior breakdown voltage allow for the creation of high-power, high-frequency devices that operate efficiently in harsh environments [39,40]. They are crucial for components in electric vehicles, fast chargers, and power grids, where they enable smaller, more efficient, and more reliable systems. For example, SiC-based transistors and diodes can handle higher temperatures and voltages than traditional silicon-based devices [41]. In photonics, SiC nanostructures are a promising platform for quantum technologies. Their unique optical properties, such as a wide transparency range from UV to infrared and the presence of stable color centers (point defects), allow them to act as single-photon emitters and spin qubits for quantum computing and sensing [42]. In multilayer structures, SiC nanostructures can be integrated with other materials to form heterostructures, such as SiC-on-insulator stacks [43,44]. These configurations are essential for creating high-quality optical cavities and waveguides that tightly confine light, facilitating a new generation of integrated photonic circuits [45,46]. This ability to be integrated into complex architectures makes SiC a foundational material for next-generation optoelectronic and quantum devices [47,48].

The aim of this research is to synthesize multilayer structures from silicon dioxide and silicon carbide thin films using DC reactive magnetron sputtering, and analyze their optoelectronic properties.

## 2. Experimental work

A DC reactive magnetron sputtering system was employed to deposit $SiO_2$ and SiC thin films onto glass or silicon substrates. Initially, a Leybold-Heraeuos rotary pump (24 $m^3$/h) established a base pressure of approximately 0.15 mbar. Prior to deposition, both the sputtering targets and the glass substrates underwent thorough cleaning and drying. The silicon target was meticulously positioned on the cathode. Plasma generation for the sputtering process was achieved through the electrical discharge of argon, powered by a high-voltage DC supply. The operational parameters of the system were categorized into constant and variable settings. Constant conditions included vacuum pressure, current limiting resistance, discharge voltage, discharge current (maintained at 35 mA), gas flow rate, deposition temperature, and inter-electrode distance (set at 4 cm). Deposition time was one hour and the $Ar:O_2$ gas mixing ratio was 50:50 while SiC thin films were prepared from sooted silicon target. The optoelectronics measurements were carried out in the spectral range of 200-1100 using a Spectra Academy SV2200 spectrophotometer with replaceable sources.

## 3. Results and discussion

Figure (1) presents the absorption spectra for two distinct heterostructures: $SiC/SiO_2$ and $SiO_2/SiC$, both prepared in this work using DC reactive sputtering. Both samples exhibit very high absorbance in the UV region, specifically below approximately 350 nm, where the absorbance values sharply increase, indicating strong absorption in this spectral range, likely due to the intrinsic absorption characteristics of both SiC and $SiO_2$. Beyond the UV region, in the visible and near-infrared (NIR) spectrum (from approximately 400 nm to 1100 nm), the two samples show a clear and consistent difference in their absorbance levels. $SiO_2/SiC$ sample consistently displays higher absorbance across the entire visible and NIR range compared to $SiC/SiO_2$ sample. For instance, at 400 nm, $SiO_2/SiC$ sample absorbance is around 1.6, while $SiC/SiO_2$ sample's is approximately 0.9. This difference persists and becomes more pronounced at longer wavelengths, with $SiO_2/SiC$ sample maintaining an absorbance above 1.0 even

 ISSN (print) 2958-8960 (online) 3006-6042 Printed in IRAQ 

at 1100 nm, whereas SiC/$SiO_2$ sample drops to around 0.6. This higher absorbance in the $SiO_2$/SiC configuration suggests that this stacking order leads to more efficient photon absorption or less reflection within the film and/or the interfaces. This could be attributed to variations in film thickness, density, stoichiometry, or surface roughness resulting from the different deposition sequences. The increased absorbance in $SiO_2$/SiC sample might correlate with its superior photoresponse (as seen in EQE and responsivity data), indicating that a greater proportion of incident light is absorbed and converted into useful electrical signals.

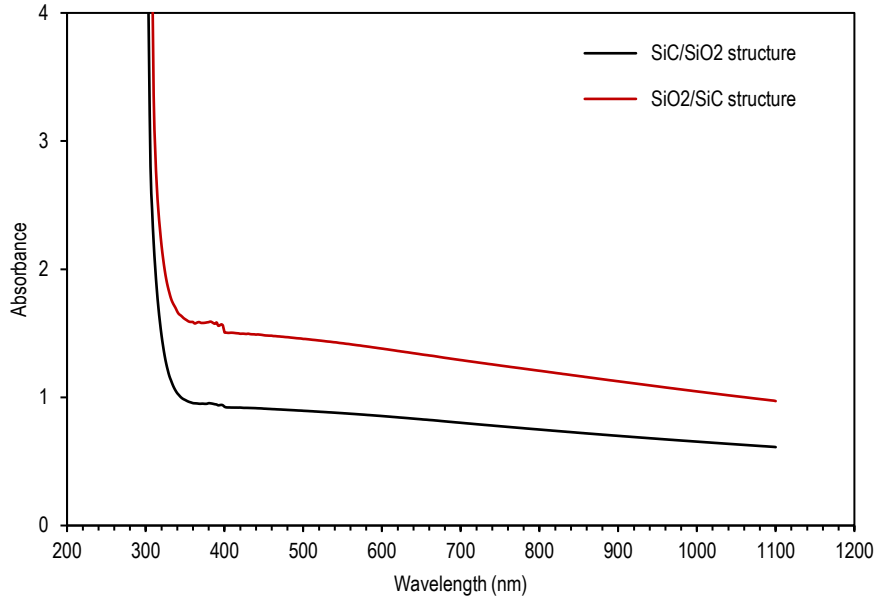


**Fig. (1) Absorption spectra of the multilayer structures fabricated in this work**

Figures (2) and (3) display photoluminescence (PL) spectra for both SiC/$SiO_2$ and $SiO_2$/SiC heterostructures, respectively, highlighting the influence of both layer stacking order and substrate material (glass vs. silicon) on their luminescent properties. All structures were prepared by DC reactive sputtering. In case of SiC/$SiO_2$ structure on glass (Fig. 2a), a relatively broad emission is shown with a prominent peak around 500-520 nm (green region) and another less intense, broader peak extending into the red-NIR region (around 700-800 nm). The overall PL intensity appears moderate, suggesting a reasonable number of radiative recombination centers within the SiC/$SiO_2$ film when deposited on a transparent glass substrate. The green emission is often associated with defects or quantum confined states in SiC or at the SiC/$SiO_2$ interface. In case of the same structure on silicon substrate (Fig. 2b), the overall PL intensity is significantly lower compared to the same structure on glass. While a broad emission band is still present, possibly peaking around 550-600 nm, the signal is much weaker. The most striking difference is the substantial quenching of luminescence. Silicon is an indirect bandgap semiconductor and is highly absorbent in the visible and UV regions. When SiC/$SiO_2$ is deposited on silicon, a significant portion of the emitted light from the SiC/$SiO_2$ layer is likely re-absorbed by the underlying silicon substrate, leading to a drastic reduction in the detected PL signal. This quenching effect makes it challenging to discern specific peaks, but the general shape suggests a broad emission characteristic of defects within the layers or at the interfaces.

Figure (3a) for $SiO_2$/SiC structure on glass displays a very distinct and strong emission profile. It exhibits a high-intensity peak in the blue-green region, possibly around 450-500 nm, and another very prominent, broad peak extending into the red-NIR, with a peak around 700-750 nm. The overall PL intensity is considerably higher than both SiC/$SiO_2$ structures, especially compared to the one on silicon. The $SiO_2$ layer on top might be acting as a protective or passivating layer for the SiC, reducing non-radiative recombination and allowing for more efficient light emission, particularly in the longer wavelength range. The glass substrate, being transparent, ensures minimal re-absorption of the emitted light. Figure (3b) for the same structure on silicon substrate, similar to the SiC/$SiO_2$ on silicon, also shows significantly quenched luminescence compared to its counterpart on glass. The spectrum is characterized by very low intensity, with a broad, ill-defined peak somewhere in the green-yellow region (around 550 nm). The presence of the silicon substrate once again dominates the optical response by

absorbing the emitted photons, leading to a substantial reduction in the detected PL signal. Despite the difference in layer order compared to the second figure, the fundamental limitation imposed by the silicon substrate's absorption characteristics remains dominant, masking the intrinsic luminescence of the $SiC/SiO_2$ stack.

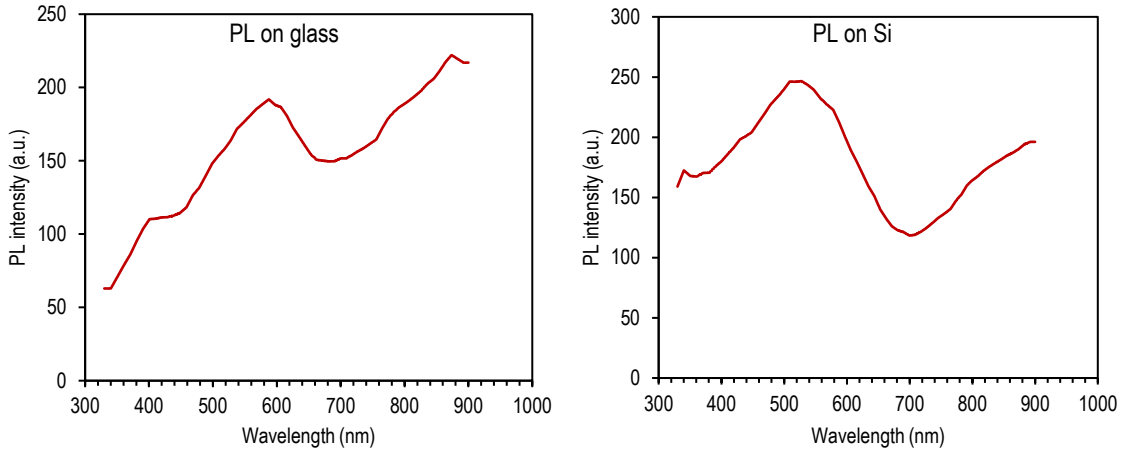


**(a)** **(b)**

**Fig. (2) Photoluminescence spectra of the $SiC/SiO_2$ structure on glass (a) and on silicon substrate (b)**

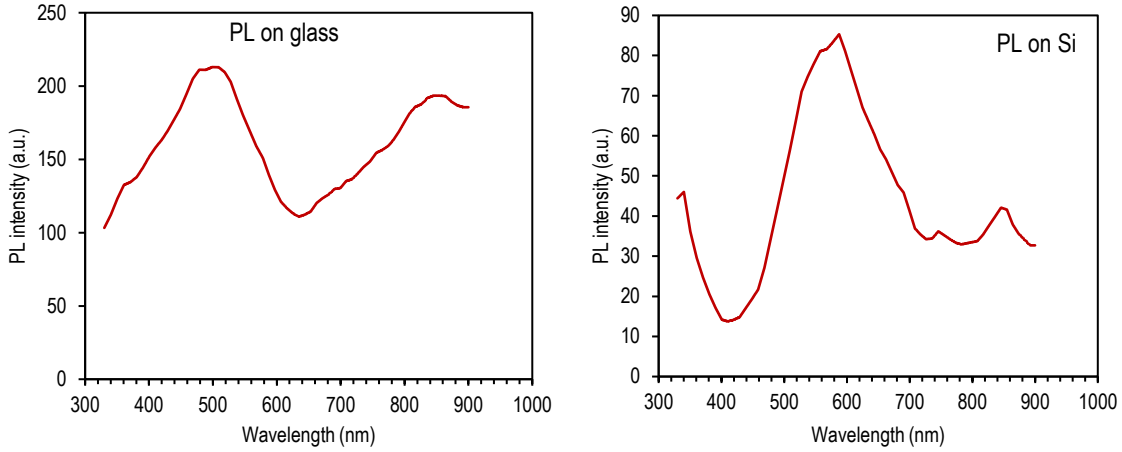


**Fig. (3) Photoluminescence spectra of the $SiO_2/SiC$ structure on glass (a) and on silicon substrate (b)**

The choice of substrate plays a paramount role in the observed PL intensity, with silicon substrates drastically quenching the luminescence due to re-absorption, making direct comparison of intrinsic layer properties challenging for silicon-based samples. Glass substrates, being transparent, allow the intrinsic luminescence of the thin films to be clearly observed. Between the glass-based samples, the $SiO_2/SiC$ stacking yields significantly higher PL intensity and different spectral characteristics compared to the $SiC/SiO_2$ stacking. This suggests that the order of deposition, and consequently the interface formed between SiC and $SiO_2$, critically influences the density and nature of luminescent defects and non-radiative recombination pathways. The $SiO_2$ deposited on SiC appears to create a more favorable environment for efficient photoluminescence compared to SiC on $SiO_2$.

Figures (4) and (5) display the current-voltage (I-V) characteristics of the two heterostructures: $SiC/SiO_2$ (Fig. 4a) and $SiO_2/SiC$ (Fig. 5a). A comparison of these I-V curves reveals significant differences in their electrical behavior, particularly in terms of current magnitude, rectification, and symmetry. Figure (4a) shows a highly rectifying behavior. In forward bias, the current increases sharply, reaching over 600μA at 5V. In reverse bias, the current remains very low, staying close to zero and only reaching approximately −10μA at -5V. This strong rectification, with high current flow in forward bias and minimal leakage in reverse bias, indicates the formation of a good quality p-n or Schottky junction, where the $SiO_2$ layer might be acting as a passivation or tunneling layer rather than a thick insulating barrier. The current onset in forward bias appears to be around 0.5-1V. In contrast, figure (5a) exhibits a much lower current magnitude across both forward and reverse biases. The maximum current in forward bias

at 5V is approximately 40μA, which is significantly lower than the SiC/$SiO_2$ structure. In reverse bias, the current is also very low, reaching about −7μA at -5V. While some rectification is still present, the overall current levels are considerably reduced compared to the first figure. This suggests that in the $SiO_2$/SiC configuration, the $SiO_2$ layer likely acts as a more substantial insulating barrier, limiting current flow in both directions. The different ordering of the layers (i.e., SiC on $SiO_2$ versus $SiO_2$ on SiC) significantly impacts the interface properties, defect states, and effective barrier heights, leading to these distinct electrical transport characteristics. The much higher current in the SiC/$SiO_2$ configuration might imply a lower series resistance or a different band alignment at the interface facilitating charge transport.

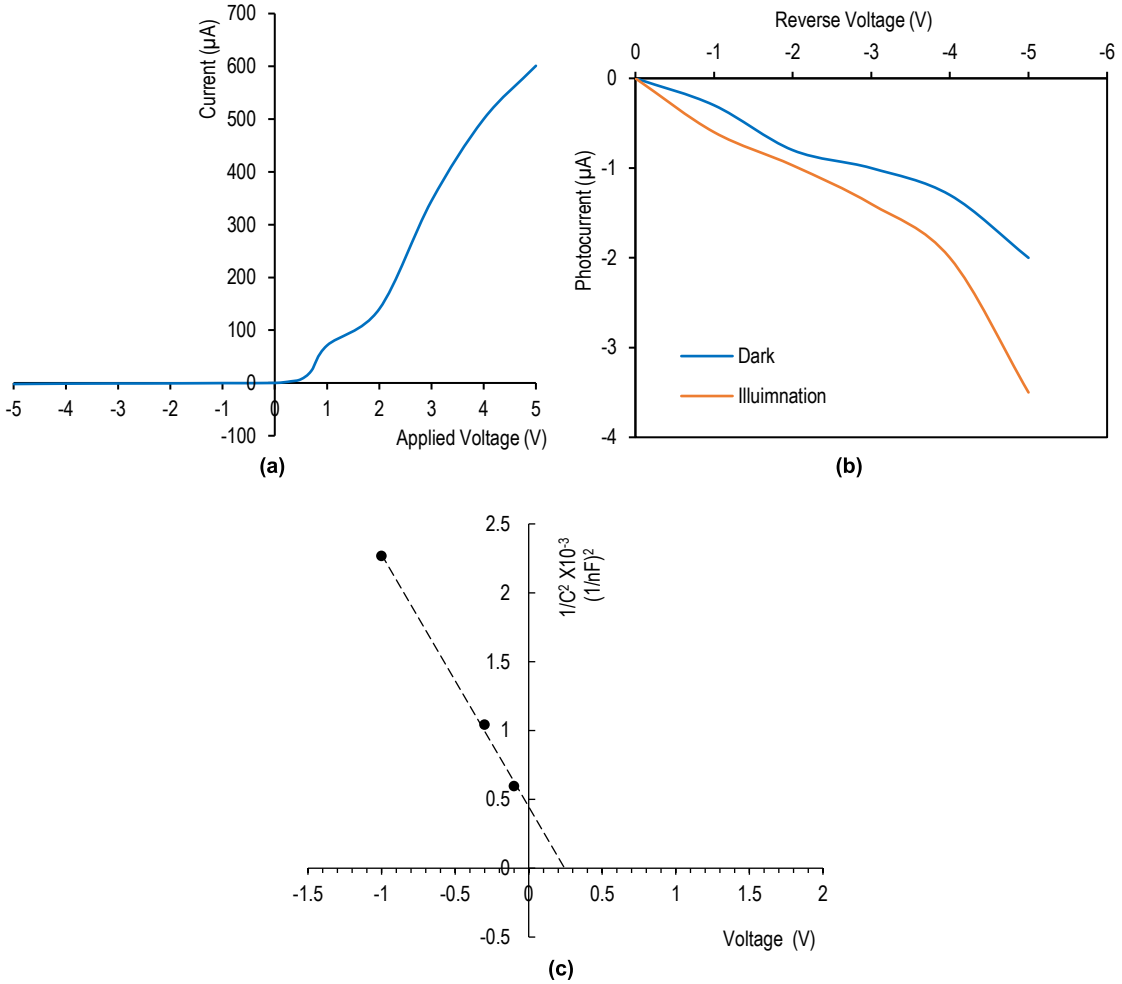


**Fig. (4) Electrical characteristics of the SiC/$SiO_2$ structure (a) I-V characteristics in dark, (b) photocurrent in dark and illumination, and (c) 1/$C^2$ versus applied voltage**

Figures (4b) and (5b) illustrate the photocurrent variation with reverse applied voltage for the two heterostructures. A direct comparison reveals significant differences in their photoresponse characteristics under dark and illuminated conditions. For the SiC/$SiO_2$ structure (Fig. 4b), the dark current remains very low, approaching approximately −2μA at -5.5V, indicating good insulation and low leakage. Upon illumination, the photocurrent significantly increases, reaching about −3.5μA at -5.5V. This clear separation between dark and illuminated current, coupled with a notable increase in current under light, demonstrates a strong photoresponse and effective photocarrier generation and collection. The device acts as an efficient photodetector in this configuration. In contrast, the $SiO_2$/SiC structure (Fig. 5b) exhibits a much higher dark current and a less pronounced relative increase in photocurrent upon illumination. The dark current reaches approximately −70μA at -5.5V, which is substantially higher than that of the SiC/$SiO_2$ structure. Under illumination, the current increases to about −135μA at -5.5V. While there is still a photoresponse, the high dark current limits the overall signal-to-noise ratio and hence the detectivity. This suggests that the $SiO_2$ layer, when placed on top of the SiC in this configuration, might introduce more defects or create a less ideal interface for blocking dark current, or


ISSN (print) 2958-8960 (online) 3006-6042 Printed in IRAQ

it could be due to a different band alignment that leads to higher leakage. The difference in layer ordering profoundly affects the electrical transport and photovoltaic properties of the heterojunction.

Figures (4c) and (5c) display 1/C2 (reciprocal of squared capacitance) versus applied voltage (C-V characteristics in Mott-Schottky plot form) for the two These plots are crucial for understanding the doping concentration of the semiconductor and the built-in potential of the junction. For the SiC/$SiO_2$ structure (Fig. 4c), the $1/C^2$ values are significantly higher, ranging from approximately $0.5\times10^{-3}$ to $2.3\times10^{-3}$ ($1/nF^2$). The data points show a clear linear relationship in the reverse bias region (negative voltage), which is characteristic of a Schottky or p-n junction. The slope of this linear region can be used to determine the doping concentration of the semiconductor, while the x-intercept (where $1/C^2=0$) provides the built-in potential of the junction. The relatively higher $1/C^2$ values suggest a lower capacitance, which could imply a thicker depletion region or lower doping concentration in the SiC side of the SiC/$SiO_2$ structure. In contrast, the $SiO_2$/SiC structure (Fig. 5c) exhibits much lower $1/C^2$ values, ranging from approximately $0.045\times10^{-3}$ to $0.0495\times10^{-3}$ ($1/nF^2$). This indicates a significantly higher capacitance compared to the SiC/$SiO_2$ structure. The data points also appear to show a linear trend, but the range of values is much narrower. The lower $1/C^2$ values and higher capacitance suggest a thinner depletion region or a higher doping concentration in the SiC of the $SiO_2$/SiC structure. The difference in the magnitude of $1/C^2$ and potentially the slope between the two configurations highlights how the deposition sequence and resulting interface properties impact the electrical characteristics and charge distribution within the heterojunction.

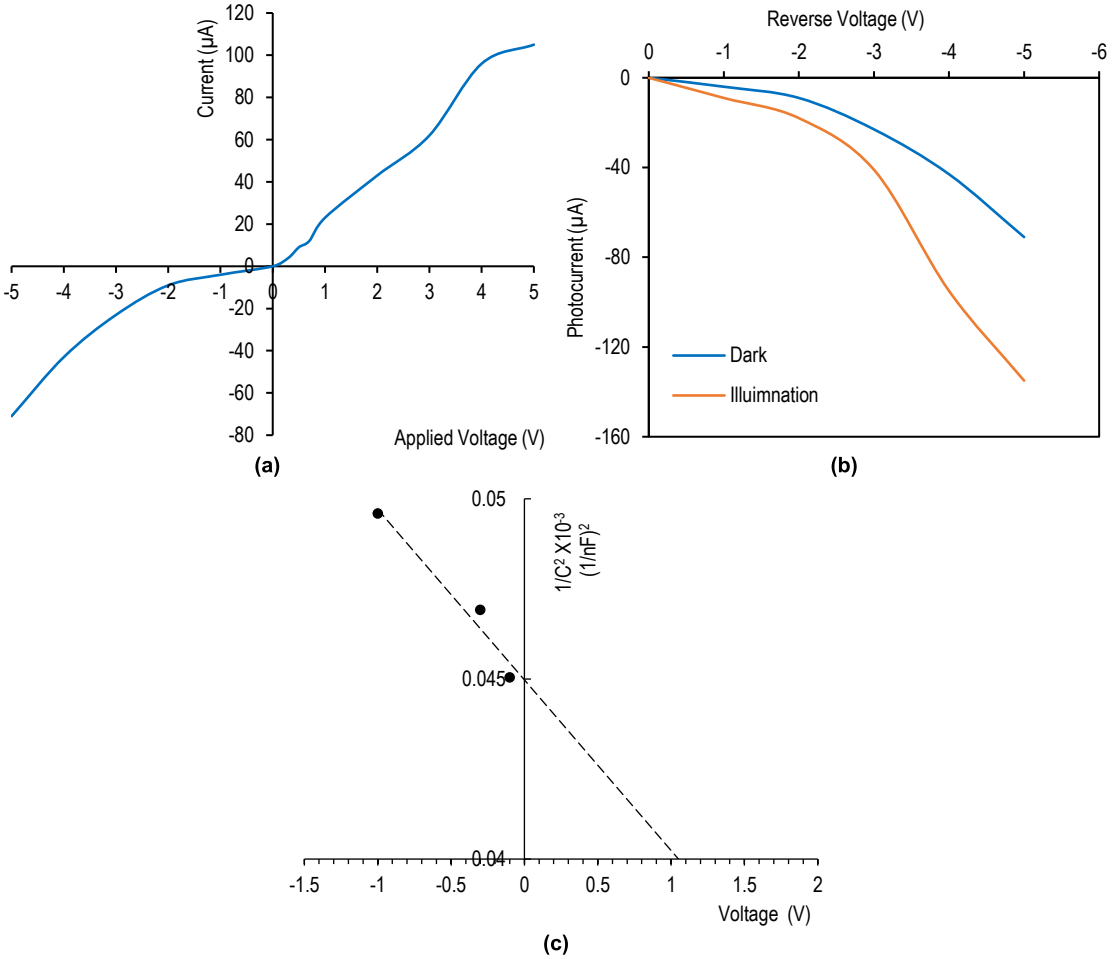


**Fig. (5) Electrical characteristics of the $SiO_2$/SiC structure (a) I-V characteristics in dark, (b) photocurrent in dark and illumination, and (c) $1/C^2$ versus applied voltage**

Figures (6a) and (7a) present the spectral responsivity (Rλ, in A/W) as a function of wavelength for the two heterostructures. A direct comparison reveals a significant difference in both the magnitude and spectral dependence of their responsivity. For the SiC/$SiO_2$ structure (Fig. 6a), the responsivity is relatively lower overall. It shows a gradual increase from approximately 0.05 A/W in the visible range


ISSN (print) 2958-8960 (online) 3006-6042 Printed in IRAQ

(around 400-500 nm) to a peak of about 0.37 A/W at around 870 nm. This suggests that the device is more sensitive to light in the near-infrared region, which is typical for silicon-based photodetectors due to silicon's bandgap. In contrast, the $SiO_2$/SiC structure (Fig. 7a) exhibits a remarkably higher responsivity across the measured spectrum. While it also shows a similar trend of increasing responsivity with wavelength, its peak responsivity reaches approximately 1.55 A/W at around 870 nm. This value is several times higher than the peak responsivity of the SiC/$SiO_2$ structure. The higher responsivity in the $SiO_2$/SiC configuration indicates a more efficient conversion of incident photons into electrical current. This could be attributed to a better interface quality between the $SiO_2$ and SiC layers in this specific stacking order, leading to reduced recombination losses and more effective collection of photogenerated carriers. The distinct spectral responsivity profiles underscore the significant impact of layer ordering on the photovoltaic performance of these heterojunction devices.

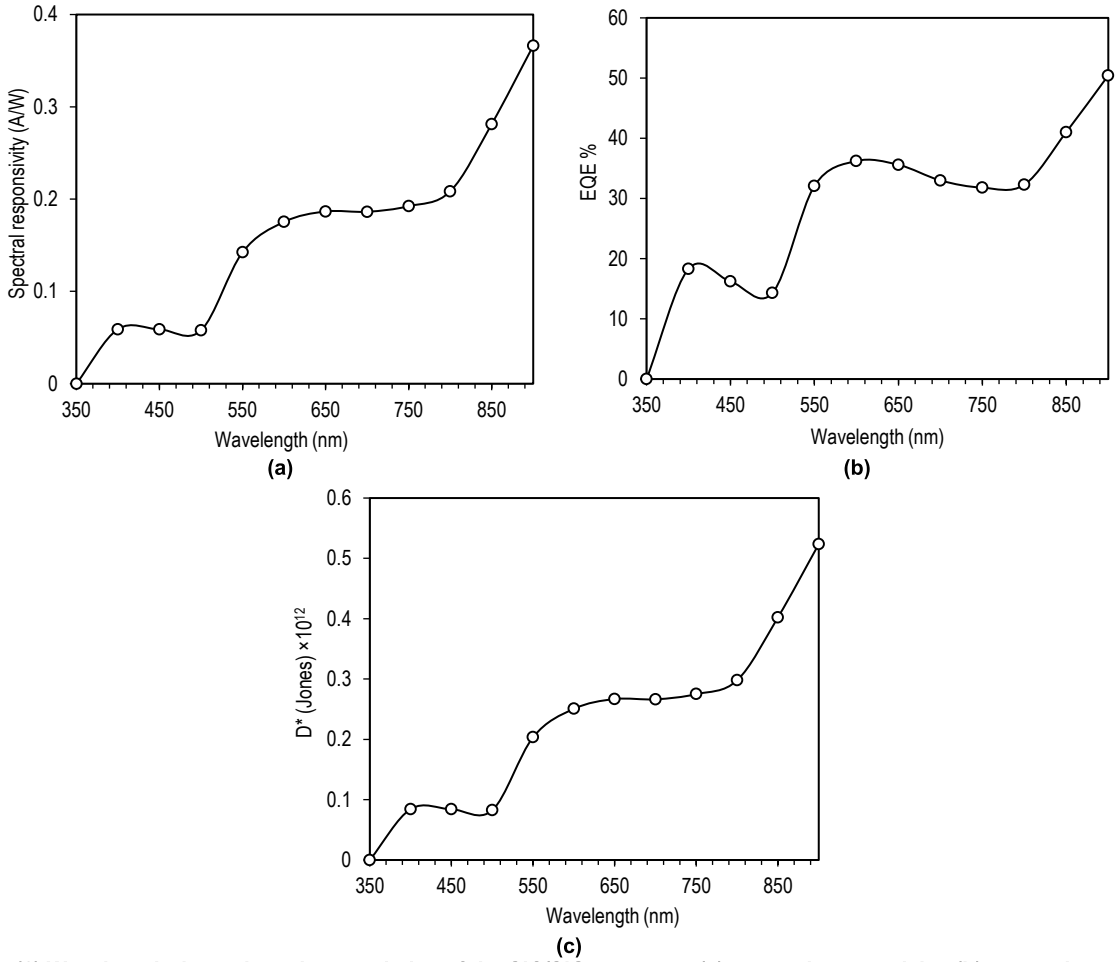


**Fig. (6) Wavelength-dependent characteristics of the SiC/$SiO_2$ structure (a) spectral responsivity, (b) external quantum efficiency, and (c) specific detectivity**

Figures (6b) and (7b) display the external quantum efficiency (EQE) as a function of wavelength for the two heterostructures. A comparison highlights significant differences in their efficiency of converting photons into electrons. For the SiC/$SiO_2$ structure (Fig. 6b), the EQE generally increases with wavelength, showing a broad response in the visible and near-infrared regions. It starts around 0% at 350 nm, rises to a peak of approximately 36% at around 580 nm, and then gradually increases again to about 50% at 900 nm. This profile suggests that the device is reasonably efficient, particularly in the longer wavelength range, which is typical for silicon-based photodetectors. The $SiO_2$/SiC structure (Fig. 7b) demonstrates a remarkably higher EQE across almost the entire spectrum. Its EQE is much higher in the visible range, reaching about 80% at 400 nm and then exhibiting a plateau around 140-150% from approximately 550 nm to 800 nm. Notably, the EQE further soars to an astonishing peak of over 200% at 900 nm. An EQE exceeding 100% indicates that the device might be exhibiting carrier multiplication phenomena, where a single incident photon generates more than one electron-hole pair. This could be

 ISSN (print) 2958-8960 (online) 3006-6042 Printed in IRAQ 

due to impact ionization or other high-energy processes occurring within the SiC or at the $SiO_2$/SiC interface. The significantly higher EQE in the $SiO_2$/SiC configuration suggests a superior design or interface quality for photodetection, allowing for more efficient photon absorption and carrier collection, possibly due to a favorable band alignment or reduced defects compared to the SiC/$SiO_2$ arrangement.

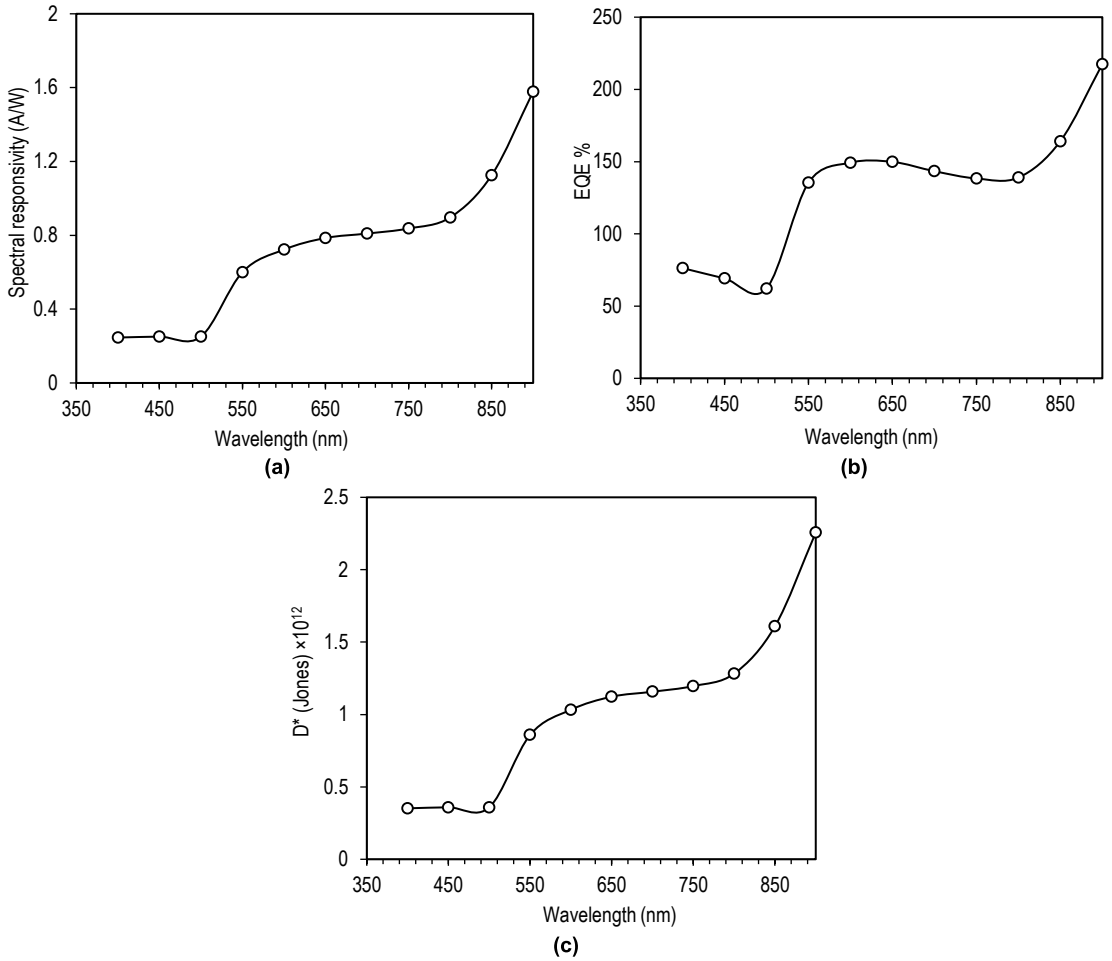


**Fig. (7) Wavelength-dependent characteristics of the $SiO_2$/SiC structure (a) spectral responsivity, (b) external quantum efficiency, and (c) specific detectivity**

Figures (6c) and (7c) display the specific detectivity ($D^*$) as a function of wavelength for the two heterostructures. A comparison reveals a stark difference in their ability to detect weak optical signals. For the SiC/$SiO_2$ structure (Fig. 6c), the detectivity is notably lower across the entire spectrum. It shows values generally ranging from approximately $0.05\times10^{12}$ Jones in the visible region to a peak of about $0.52\times10^{12}$ Jones at 870 nm. While it exhibits a clear photoresponse and spectral dependence, the overall detectivity is modest. The $SiO_2$/SiC structure (Fig. 7c) demonstrates significantly higher detectivity values. Its detectivity starts around $0.3\times10^{12}$ Jones at 380 nm, and consistently remains high, peaking at approximately $2.2\times10^{12}$ Jones at 870 nm. This value is several times higher than that of the SiC/$SiO_2$ structure. The dramatically improved detectivity in the $SiO_2$/SiC configuration suggests a superior signal-to-noise ratio, indicating a more efficient photodetector. This enhanced performance could be attributed to a combination of higher responsivity and lower noise current, possibly stemming from a better-formed junction or reduced defect states at the $SiO_2$/SiC interface compared to the reverse stacking order. The distinct detectivity profiles clearly illustrate the critical role of layer arrangement in optimizing the performance of these photodetector devices.

## 4. Conclusions

In concluding remarks, The SiC/$SiO_2$ structure shows a spectral responsivity relatively lower as this structure is more sensitive to light in the near-infrared region, which is typical for silicon-based photodetectors due to silicon's bandgap. The $SiO_2$/SiC structure demonstrates a remarkably higher EQE


ISSN (print) 2958-8960 (online) 3006-6042 Printed in IRAQ

across almost the entire spectrum reaching about 80% at 400 nm. The $SiO_2$/SiC structure demonstrates significantly higher detectivity values starting around $0.3\times10^{12}$ Jones at 380 nm, and consistently remains high, peaking at approximately $2.2\times10^{12}$ Jones at 870 nm. This value is several times higher than that of the SiC/$SiO_2$ structure. The dramatically improved detectivity in the $SiO_2$/SiC configuration suggests a superior signal-to-noise ratio, indicating a more efficient photodetector. This enhanced performance could be attributed to a combination of higher responsivity and lower noise current, possibly stemming from a better-formed junction or reduced defect states at the $SiO_2$/SiC interface compared to the reverse stacking order. The distinct detectivity profiles clearly illustrate the critical role of layer arrangement in optimizing the performance of these photodetector devices.

## References

[1] M.A. Hameed, S.H. Faisal, R.H. Turki, "Characterization of Multilayer Highly-Pure Metal Oxide Structures Prepared by DC Reactive Magnetron Sputtering Technique", Iraqi J. Appl. Phys., 16(4) (2020) 25-30
[2] M. Xu et al., "Recent advances and challenges in silicon carbide (SiC) ceramic nanoarchitectures and their applications", *Mater. Today Commun.*, 28 (2021) 102533.A.M. Hameed and M.A. Hameed, "Highly-Pure Nanostructured Metal Oxide Multilayer Structure Prepared by DC Reactive Magnetron Sputtering Technique", Iraqi J. Appl. Phys., 18(4) (2022) 9-14.
[3] M. Girardi et al., "Multilayer integration in silicon nitride: decoupling linear and nonlinear functionalities for ultralow loss photonic integrated systems", *Opt. Exp.,* 31 (2023) 31435-31446.
[4] F.K. Tareq and S. Rudra, "Enhancing the performance of silicon-based anode materials for alkali metal (Li, Na, K) ion battery: A review on advanced strategies", *Mater. Today Commun.,* 39 (2024) 108653.
[5] C. Otero, R.A. Dominguez, and A. Negrete, "Optoelectronic Response of Multilayer CuO/NiO Nanostructures Fabricated with Different Particle Size Ranges", *Iraqi J. Appl. Phys. Lett.*, 8(1) (2025) 29-32.
[6] N.V. Toan et al., "Nanoengineering silicon materials by metal-assisted chemical etching for thermal energy harvesting", *Mater. Sci. Semicond. Process.*, 195 (2025) 109622.
[7] J.M. Kahraman and M.A. Khan, "Effect of Intermediate Layer Surface Condition on Photoresponse of Multilayer GaAs-based Devices", *Iraqi J. Appl. Phys. Lett.*, 8(1) (2025) 1-4.
[8] A. M. Hameed and M. A. Hameed, "Spectroscopic characteristics of highly pure metal oxide nanostructures prepared by DC reactive magnetron sputtering technique", *Emerg. Mater.*, 6(2) (2023) 627–633.
[9] K. K. Wang, P. V. Chai, and W. L. Ang, "Introduction to Nanomaterials", *Carbon Nanostructures*, F2589 (2024) 1-15.
[10] K. Pradhan et al., "Exploration of impact of ammonia concentration on the surface morphology, optical and wettability performance of $SiO_2$ thin film", *J. Mater. Sci. Mater. Electron.*, 36(5) (2025) 1-14.
[11] L.A.J. Garvie et al., "Bonding in alpha-quartz ($SiO_2$): A view of the unoccupied states", *Am. Mineral.*, 85(5-6) (2000) 732-738.
[12] N. Li and W.Y. Ching, "Structural, electronic and optical properties of a large random network model of amorphous $SiO_2$ glass", *J. Non. Cryst. Solids*, 383 (2014) 28-32.
[13] S. Eränen, "Silicon Dioxides", in Handbook of Silicon Based MEMS Mater. Technol., (2010) pp. 137–148.
[14] D.A.P. Wardani et al., "Functional Groups, Band Gap Energy, and Morphology Properties of Annealed Silicon Dioxide ($SiO_2$)", *Egypt. J. Chem.*, 66(3) (2023) 529-535.
[15] C.A. Banciu et al., "Comparative study of the hydrophobic properties of silicon dioxide particles functionalized with different agents", *J. Optoelectron. Adv. Mater.*, 25(1-2) (2023) 89-95.
[16] T. Oyama et al., "A new layer system of anti-reflective coating for cathode ray tubes", *Thin Solid Films*, 351(1-2) (1999) 235-240.
[17] V. Bhatt and S. Chandra, "Silicon dioxide films by RF sputtering for microelectronic and MEMS applications", *J. Micromech. Microeng.*, 17(5) (2007) 1066-1077.
[18] S.W. Glunz and F. Feldmann, "$SiO_2$ surface passivation layers – a key technology for silicon solar cells", *Sol. Ener. Mater. Sol. Cells*, 185 (2018) 260-269.
[19] T.S. Chen et al., "The effect of the native silicon dioxide interfacial layer on photovoltaic characteristics of gold/p-type amorphous boron carbon thin film alloy/silicon dioxide/n-type silicon/aluminum solar cells", *Sol. Ener. Mater. Sol. Cells*, 137 (2015) 185-192.
[20] H. Jung et al., "Growth characteristics and electrical properties of $SiO_2$ thin films prepared using plasma-enhanced atomic layer deposition and chemical vapor deposition with an aminosilane precursor", *J. Mater. Sci.*, 51(11) (2016) 5082-5091.
[21] M.A. Hameed and Z.M. Jabbar, "Surface Morphology and Topography of Silicon Dioxide Nanostructures Prepared by DC Reactive Sputtering", *Iraqi J. Appl. Phys. Lett.*, 7(3) (2024) 23-26.
[22] M. Yu et al., "Comparative study of the characteristics of Ni films deposited on $SiO_2$/Si(100) by oblique-angle sputtering and conventional sputtering", *Thin Solid Films*, 516(21) (2008) 7903-7909.
[23] E.S.M. Goh et al., "Thickness effect on the band gap and optical properties of germanium thin films", *J. Appl. Phys.*, 107(2) (2010) 1-5.
[24] M. Henini, **"Handbook of Thin-Film Deposition Processes and Techniques"**, 2nd ed., William Andrew Inc. (2001), vol. 31, no. 3.
[25] V. Jokanovic et al., "Thin films of SiO2 and hydroxyapatite on titanium deposited by spray pyrolysis", *J. Mater. Sci. Mater. Med.*, 19(5) (2008) 1871-1879.
[26] W. Zhang et al., "Preparation of $SiO_2$ anti-reflection coatings by sol-gel method", *Energy Procedia*, 130 (2017) 72-76.
[27] G. Wang et al., "Preparation methods and application of silicon oxide films", *Int. Conf. Mechatronics, Electron. Ind. Control Eng. MEIC 2014*, pp. 479–483.
[28] S. Chen et al., "Vanadium oxide thin films deposited on silicon dioxide buffer layers by magnetron sputtering", *Thin Solid Films*, 497(1-2) (2006) 267-269.
[29]] O.A. Hammadi, "Conjunctional Freezing-Assisted Ultrasonic Extraction of Silicon Dioxide Nanopowders from Thin Films Prepared by Physical Vapor Deposition Technique", *Iraqi J. Appl. Phys.*, 15(4) (2019) 23-28.
[30] I. Safi, "Recent aspects concerning DC reactive magnetron sputtering of thin films: A review", *Surf. Coat. Technol.*, 127(2-3) (2000) 203-218.
[31] N.H. Mutesher and F.J. Kadhim, "Comparative Study of Structural and Optical Properties of Silicon Dioxide Nanoparticles

 

Prepared by DC Reactive Sputtering and Sol-Gel Route", *Iraqi J. Appl. Phys.*, 17(1) (2021) 17-20.
[32] F.J. Kadhim et al., "Photocatalytic activity of $TiO_2/SiO_2$ nanocomposites synthesized by reactive magnetron sputtering technique", *J. Nanophot.*, 16(2) (2022) 026005 DOI: 10.1117/1.JNP.16.026005
[33] K. Pfeiffer et al., "Comparative study of ALD $SiO_2$ thin films for optical applications", *Opt. Mater. Exp.*, 6(2) (2016) 660.
[34] M.D. Beltrán et al., "Double laser for depth measurement of thin films of ice," *Sensors (Switzerland)*, 15(10) (2015) 25123-25138.
[35] H.G. Fahad and O.A. Hammadi, "Characterization of Highly-Pure Silicon Dioxide Nanoparticles as Scattering Centers for Random Gain Media", *Iraqi J. Appl. Phys.*, 16(2) (2020) 37-42.
[36] K. Praweerawat, C. Muangphat, and C. Luangchaisri, "The Preparation and Characterization of $SiO_2$ Films by Spray Coating Technique for Radiative Cooling Glass Application", *Mater. Today Proc.*, 23 (2018) 696-702.
[37] C.H. Wang, L.Q. Yang, and D.Z. Wu, "Effect of Quantum Dots Density on Response Time of Photodetectors Fabricated from Quantum Dots Deposited on Porous Indium Arsenide Layers", *Iraqi J. Appl. Phys. Lett.*, 8(1) (2025) 13-16.
[38] M.A. Hameed and Z.M. Jabbar, "Optimization of Preparation Conditions to Control Structural Characteristics of Silicon Dioxide Nanostructures Prepared by Magnetron Plasma Sputtering", *Silicon*, 10(4) (2018) 1411-1418.
[39] O.A. Hamadi, K.Z. Yahiya and O.N.S. Jassim, "Properties of Silicon Carbide Thin Films Deposited by Vacuum Thermal Evaporation", *J. Semicond. Technol. Sci.*, 5(3) (2005) 182-186.
[40] O.A. Hammadi, "Magnetically-Supported Electrically-Induced Formation of Silicon Carbide Nanostructures on Silicon Substrate for Optoelectronics Applications", *Opt. Quantum Electron.*, 54(7) (2022) 427.
[41] D.A. Taher and M.A. Hameed, "Employment of Silicon Nitride Films Prepared by DC Reactive Sputtering Technique for Ion Release Applications", *Iraqi J. Phys.*, 21(3) (2023) 33-40.
[42] O.A. Hamadi, "Characterization of SiC/Si Heterojunction Fabricated by Plasma-Induced Growth of Nanostructured Silicon Carbide Layer on Silicon Surface", *Iraqi J. Appl. Phys.*, 12(2) (2016) 9-13.
[43] R.H. Turki and M.A. Hameed, "Spectral and Electrical Characteristics of Nanostructured $NiO/TiO_2$ Heterojunction Fabricated by DC Reactive Magnetron Sputtering", *Iraqi J. Appl. Phys.*, 16(3) (2020) 39-42.
[44] A.N. Munif and F.J. Kadhim, "Structural Characteristics and Photocatalytic activity of $TiO_2/Si_3N_4$ nanocomposite synthesized via plasma sputtering technique", *Iraqi J. Phys.*, 22(4) (2024) 99-106.
[45] P. Carvalho et al., "Influence of the chemical and electronic structure on the electrical behavior of zirconium oxynitride films", *J. Appl. Phys.*, 103(10) (2008) doi: 10.1063/1.2927494.
[46] M.O. Yusuf, "Bond Characterization in Cementitious Material Binders Using Fourier-Transform Infrared Spectroscopy", *Appl. Sci.*, 13(5) (2023) doi: 10.3390/app13053353.
[47] K.A. Al-Hamdani, "Current–voltage and capacitance-voltage characteristics of Se/Si heterojunction prepared by DC planar magnetron sputtering technique", *Iraqi J. Phys.*, 8(13) (2010) 97-100.
[48] K.A. Aadim, "Control the deposition uniformity using ring cathode by DC discharge technique", *Iraqi J. Phys.*, 15(32) (2017) 57-60.

 ISSN (print) 2958-8960 (online) 3006-6042 Printed in IRAQ 